Pseudouridine residues as substrates for serum ribonucleases

CLAIR S. GUTIERREZ,^{1,2,5} BJARNE SILKENATH,^{1,5} VOLGA KOJASOY,^{1,5} JAROSLAW A. PICH,¹ DANIEL C. LIM,³ and RONALD T. RAINES^{1,2,4}

ABSTRACT

In clinical uses, RNA must maintain its integrity in serum that contains ribonucleases (RNases), especially RNase 1, which is a human homolog of RNase A. These omnipresent enzymes catalyze the cleavage of the $P-O^5$ bond on the 3' side of pyrimidine residues. Pseudouridine (Ψ) is the most abundant modified nucleoside in natural RNA. The substitution of uridine (U) with Ψ or N^1 -methylpseudouridine ($m^1\Psi$) reduces the immunogenicity of mRNA and increases ribosomal translation, and these modified nucleosides are key components of RNA-based vaccines. Here, we assessed the ability of RNase A and RNase 1 to catalyze the cleavage of the $P-O^5$ bond on the 3' side of Ψ and $m^1\Psi$. We find that these enzymes catalyze the cleavage of UpA up to 10-fold more efficiently than the cleavage of Ψ pA or $m^1\Psi$ pA. X-ray crystallography of enzyme-bound nucleoside 2',3'-cyclic vanadate complexes and molecular dynamics simulations of enzyme-dinucleotide complexes show that U, Ψ , and $m^1\Psi$ bind to RNase A and RNase 1 in a similar manner. Quantum chemistry calculations suggested that the higher reactivity of UpA is intrinsic, arising from an inductive effect that decreases the pK_a of the 2'-hydroxy group of U and enhances its nucleophilicity toward the $P-O^5$ bond. Experimentally, we found that UpA does indeed undergo spontaneous hydrolysis faster than does $m^1\Psi$ pA. Our findings reveal a new role for natural pseudouridine residues and inform the continuing development of RNA-based vaccines and therapeutic agents.

Keywords: X-ray crystallography; enzymology; inductive effect; molecular dynamics simulations; nucleoside 2',3'-cyclic vanadate

INTRODUCTION

Katalin Karikó and Drew Weissman were awarded the 2023 Nobel Prize in Physiology or Medicine for their discovery of nucleobase modifications that led to effective messenger RNA (mRNA) vaccines against COVID-19 (Krammer and Palese 2024). These modifications overcome an immune response elicited by unmodified mRNA (Weissman et al. 2000; Sahin et al. 2014; Damase et al. 2021) that could have evolved as a defense mechanism against viral RNA (Chen et al. 2021). Endosomal Toll-like receptors are responsible for this response (Karikó et al. 2004, 2005), and Karikó and Weissman discovered that replacing uridine (U) with pseudouridine (Ψ) enabled synthetic mRNAs to evade the receptors while enhancing ribosomal translation

(Karikó et al. 2005, 2008, 2011; Anderson et al. 2010; Morais et al. 2021).

U and Ψ residues form similar hydrogen bonds with adenosine residues in canonical Watson–Crick–Franklin base pairs (Fig. 1). In addition, Ψ can donate an additional hydrogen bond in the major groove, enabling enhanced local RNA nucleobase stacking, which is amplified by neighboring nucleosides (Charette and Gray 2000; Hudson et al. 2013; Kierzek et al. 2013; Spenkuch et al. 2014). The methylation of Ψ at N^1 to provide N^1 -methylpseudouridine (m $^1\Psi$) obviates the additional hydrogen bond but elicits more protein production than Ψ and further diminishes the immunogenicity (Andries et al. 2015; Svitkin et al. 2017; Parr et al. 2020). Ultimately, m $^1\Psi$ was used in most of the 14 billion administered doses of the

Handling editor: Eric Phizicky

© 2025 Gutierrez et al. This article is distributed exclusively by the *RNA* Society for the first 12 months after the full-issue publication date (see http://majournal.cshlp.org/site/misc/terms.xhtml). After 12 months, it is available under a Creative Commons License (Attribution-NonCommercial 4.0 International), as described at http://creativecommons.org/licenses/by-nc/4.0/.

¹Department of Chemistry, Massachusetts Institute of Technology, Cambridge, Massachusetts 02139, USA

²Broad Institute of MIT and Harvard, Cambridge, Massachusetts 02143, USA

³Department of Biology, Massachusetts Institute of Technology, Cambridge, Massachusetts 02139, USA

 $^{^4}$ Koch Institute for Integrated Cancer Research at MIT, Cambridge, Massachusetts 02139, USA

⁵These authors contributed equally to this work. **Corresponding author: rtraines@mit.edu**

Article is online at http://www.majournal.org/cgi/doi/10.1261/rna .080404.125.

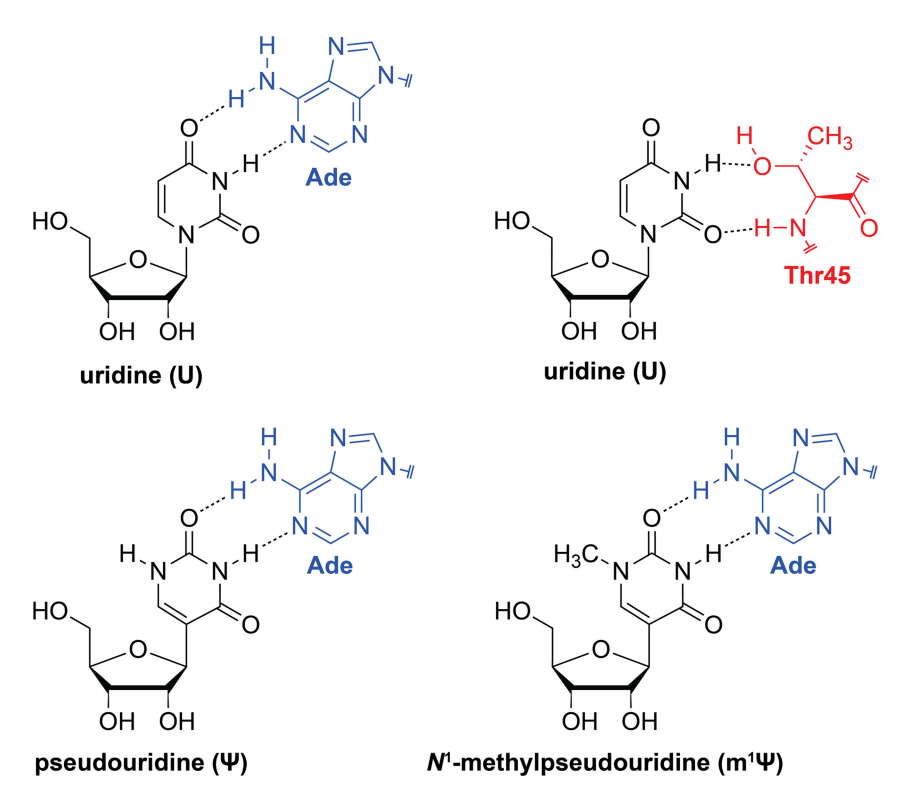


FIGURE 1. Structure of U, Ψ , and m¹ Ψ , their base-pairing with adenine (Ade), and the interaction of U with Thr45 of ptRNases.

COVID-19 vaccine (Nance and Meier 2021; Vogel et al. 2021; Demongeot and Fougère 2022).

 Ψ , which is the C^5 -glycoside isomer of U, was discovered in 1951 as the first post-transcriptional modification in RNA (Cohn and Volkin 1951). Today, Ψ is known to be the most abundant modified nucleoside and is found in RNA from all domains of life (Spenkuch et al. 2014). Ψ is enriched in the coding sequence and 3'-untranslated regions of mRNAs (Carlile et al. 2014; Schwartz et al. 2014; Karijolich et al. 2015; Li et al. 2015; Cerneckis et al. 2022). In nearly all transfer RNAs (tRNAs), Ψ is found in the TYC stem-loop (and elsewhere) and can stabilize tRNA conformation (Charette and Gray 2000; Motorin and Helm 2010; Guzzi et al. 2018). Ψ accounts for 1.4% of all nucleosides in human ribosomal RNA (rRNA) and modulates its conformational dynamics (Jiang et al. 2015; Penzo and Montanaro 2018; Cerneckis et al. 2022). $m^{1}\Psi$ is also a natural nucleoside but is much less common than Ψ (Wurm et al. 2012).

Surprisingly little is known about Ψ or $m^1\Psi$ as substrates for ribonucleases (RNases). Ψ does impede the ability of human RNase L (Anderson et al. 2011) and bacterial RNase E (Islam et al. 2021) to degrade RNA. Yet, no analyses have been performed with pancreatic-type RNases (ptRNases). These secretory enzymes are by far the most abundant and active RNases in humans and other vertebrates (Green and Sambrook 2019; Sun et al. 2022), and

are of utmost concern for the integrity of extracellular RNA (Wang et al. 2021). In ptRNases, a conserved residue, Thr45 (Fig. 1), forms hydrogen bonds with pyrimidine residues in an RNA substrate and precludes the binding of purine residues (delCardayré and Raines 1994, 1995; Kelemen et al. 2000).

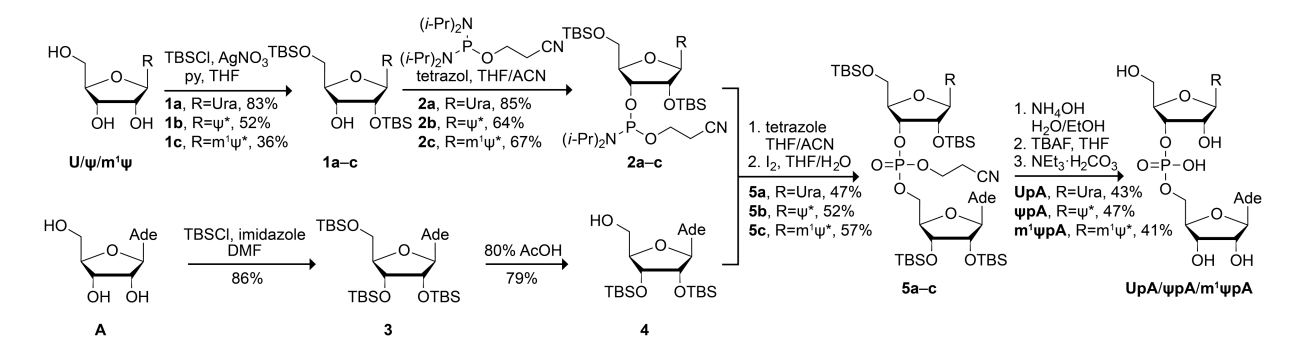
Here, we report on Ψ and $m^1\Psi$ as substrates for ptRNases. We focus our analyses on two homologs: (1) bovine pancreatic ribonuclease (RNase A), which served as a model protein for seminal studies in biological chemistry during the twentieth century (D'Alessio and Riordan 1997; Raines 1998: Marshall et al. 2008). and (2) human ribonuclease 1 (RNase 1), which is the most abundant ribonuclease in human serum and has especially high catalytic activity (Lomax et al. 2017; Garnett and Raines 2022). We investigate the kinetics of the enzyme-catalyzed and uncatalyzed cleavage of synthetic dinucleotide substrates: uridylyl (3'→5')adenosine (UpA), pseudouri-

dylyl(3' \rightarrow 5')adenosine (Ψ pA), and N^1 -methylpseudouridylyl(3' \rightarrow 5')adenosine ($m^1\Psi$ pA). To correlate structure and function, we deploy X-ray crystallography to obtain highresolution structures of RNase A complexed with the 2',3'-cyclic vanadyl diesters of U, Ψ , and $m^1\Psi$. To gain structural insight into substrate binding, we carried out molecular dynamics (MD) simulations of RNase 1 complexes with UpA, Ψ pA, and $m^1\Psi$ pA. Finally, we examined the intrinsic stability of UpA, Ψ pA, and $m^1\Psi$ pA. The ensuing data provide guidance for the development of RNA-based vaccines and therapeutic agents, along with new insight about the most common post-transcriptional modification.

RESULTS

Synthesis of dinucleotide substrates

ptRNases catalyze the cleavage of the $P-O^{5''}$ bond in RNA between a pyrimidine residue and (preferentially) a purine residue (Fontecilla-Camps et al. 1994; Zegers et al. 1994). UpA has been the most often used dinucleotide substrate, and its cleavage forms uridine 2',3'-cyclic phosphate and adenosine (Cuchillo et al. 1993; Thompson et al. 1994). An ensuing change in UV absorption enables the facile determination of steady-state kinetic parameters (Witzel and Barnard 1962). Reasoning that ΨpA and $m^1 \Psi pA$ would also be amenable to this assay, we synthesized UpA,



SCHEME 1. Synthetic route to UpA, Ψ pA, and m¹ Ψ pA. Ψ * = a pseudouracil nucleobase.

 Ψ pA, and m¹ Ψ pA from their component nucleosides by using the phosphoramidite method (Scheme 1; Caruthers 2011).

Briefly, AgNO₃-mediated silylation allowed for the synthesis of the three 5'- and 2'-silyl-protected nucleosides **1a-c** (Stowell et al. 1995). The reaction of the 3'-hydroxy group with 2-cyanoethyl tetraisopropylphosphorodiamidite and tetrazole gave phosphoramidites **2a-c**. 2',3'-Silyl-protected adenosine 4 was accessed by the protection of the three hydroxy groups of adenosine with TBS to provide **3**, followed by selective 5' deprotection in aqueous acetic acid (Ogilvie et al. 1978).

Activating phosphoramidites 2a-c with tetrazole and coupling with 4, followed by oxidation with iodine, gave protected dinucleotides 5a-c. β -Elimination of the cyanoethyl groups with ammonium hydroxide, followed by silyl ether deprotection with tetrabutylammonium fluoride and purification by anion-exchange chromatography, gave UpA, Ψ pA, and $m^1\Psi$ pA as triethylammonium salts.

Heterologous production of RNase 1

Human RNase 1 was produced in *Escherichia coli* by recombinant DNA technology as described previously (Ressler et al. 2019). Both purified RNase 1 (Supplemental Fig. S1) and RNase A (which was obtained from a commercial vendor) catalyzed the cleavage of a model substrate, FAM–dArUdAdA–6-TAMRA (Supplemental Fig. S2), with $k_{\rm cat}/K_{\rm M}$ values similar to those in the literature (Supplemental Table S1).

UpA, Ψ pA, and m¹ Ψ pA as substrates for RNase A and RNase 1

Catalysis of UpA, ΨpA, and m¹ΨpA was assayed by using UV spectroscopy. The UV spectra of UpA, ΨpA, and m¹ΨpA are similar, though that of m¹ΨpA is shifted slightly to higher wavelengths (Supplemental Fig. S3). To assess the three dinucleotides as substrates for ptRNases, we sought changes in absorbance near 280 nm that accompany dinucleotide cleavage (Witzel and Barnard 1962). Those

changes were apparent, albeit small (Supplemental Fig. S4), and we chose an optimal wavelength for monitoring each cleavage reaction (Supplemental Table S2). We performed assays at the optimal pH for catalysis by RNase A (pH 6.0) and RNase 1 (pH 7.5), which reflects their physiological environments (Lomax et al. 2017).

We found that all three dinucleotides are substrates for both RNase A and RNase 1 (Supplemental Fig. S5). Plots of the initial rates are shown in Figure 2, and steady-state kinetic parameters are listed in Table 1. In general, UpA is a better substrate than either ΨpA or $m^1 \Psi pA$. The differences, which are more significant for RNase A, are due

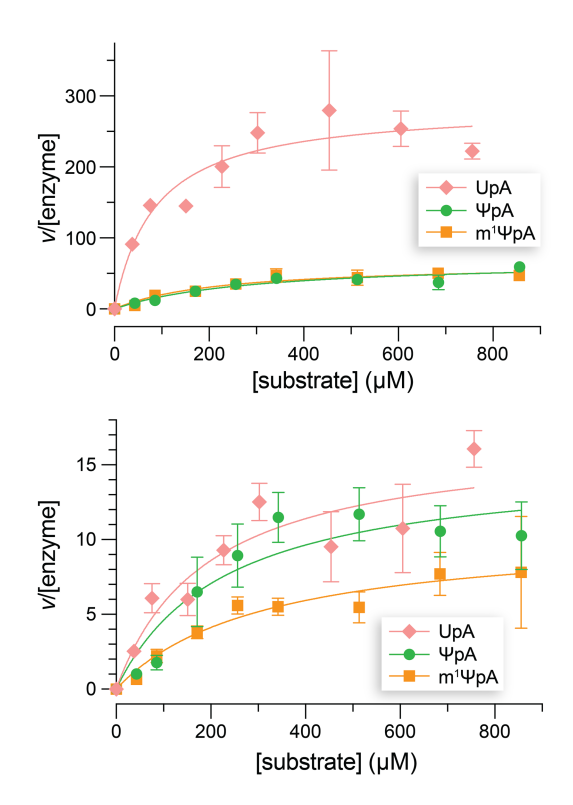


FIGURE 2. Initial rates for catalysis of the cleavage of dinucleotide substrates by RNase A (pH 6.0) and RNase 1 (pH 7.5) at 25° C. Values are the mean \pm SD of four replicates. The resultant steady-state kinetic parameters are listed in Table 1.

TABLE 1. Steady-state kinetic parameters for the cleavage of UpA, Ψ pA, and m¹ Ψ pA by RNase A and RNase 1

Enzyme	рН	Substrate	$k_{\rm cat}$ (sec ⁻¹)	<i>K</i> _M (μM)	$k_{\rm cat}/K_{\rm M}~(10^5~{ m M}^{-1}~{ m sec}^{-1})$
RNase A	6.0	UpA	313 ± 25	143 ± 39	21.8 ± 6.2
	6.0	ΨрА	65 ± 7	305 ± 84	2.1 ± 0.6
	6.0	m¹ΨpA	70 ± 7	300 ± 82	2.3 ± 0.7
RNase 1	7.5	UpA	17 ± 2	253 ± 77	0.67 ± 0.22
	7.5	ΨрА	14 ± 2	254 ± 88	0.58 ± 0.21
	7.5	m¹ΨpA	9 ± 1	328 ± 116	0.30 ± 0.12

primarily to decreases in the value of $k_{\rm cat}$ rather than changes in the value of $K_{\rm M}$. The largest differences are nearly 10-fold, which are for the $k_{\rm cat}/K_{\rm M}$ values of RNase A. UpA is also a better substrate than either Ψ pA or ${\rm m}^1\Psi$ pA at the pH optimum of the other enzyme, that is, RNase A at pH 7.5 and RNase 1 at pH 6.0 (Supplemental Table S3; Supplemental Fig. S6).

Structural interactions of U, Ψ , and $m^1\Psi$ with RNase A

Next, we sought to understand the basis for the decrease in catalytic efficiency for the cleavage of Up Ψ and Upm¹ Ψ versus UpA. To do so, we focused initially on structure. Uridine 2',3'-cyclic vanadate (U > v) is a potent inhibitor of RNase A, superior to uridine or inorganic vanadate alone (Lindquist et al. 1973). This complex is thought to be a mimic of the enzymic transition state, albeit an imprecise one (Krauss and Basch 1992; Messmore and Raines 2000b). Given that precedent, we sought and obtained crystal structures of RNase A bound to U > v, $\Psi > v$, and $m^{1}\Psi > v$, which we solved at resolutions of 1.83, 1.70, and 1.71 Å, respectively. The data and refinement statistics for each structure are listed in Supplemental Table S4. In these structures, we found that each vanadyl group is in a tetrahedral geometry (Supplemental Fig. S7), instead of the previously reported trigonal bipyramidal geometry (Wlodawer et al. 1983; Ladner et al. 1997). Thus, the crystal structures mimic the enzymic complex with the 2',3'-cyclic phosphodiester product of the reaction rather than the transition state. That lower valency, however, did not alter the location of the uridine moiety. In addition, we observed decavanadates in each crystal lattice (Supplemental Fig. S8). This byproduct of the nucleoside plus vanadate complexation reaction is likewise known to be an inhibitor of catalysis by RNase A (Messmore and Raines 2000a), though its structural interaction with the enzyme had not been described previously.

An overlay of the U > v, Ψ > v, and $m^1\Psi$ > v moieties bound to RNase A is shown in Figure 3. The binding of

the ligand is virtually identical in the three structures. Specifically, each uridine ring is in the *anti* conformation and interacts with Thr45 in a similar manner. The near-identity of these three structures suggests that the observed differences in steady-state kinetic parameters (Table 1) do not arise primarily from structural differences.

Simulation of RNase 1 binding to UpA, Ψ pA, and m¹ Ψ pA

We were unable to obtain the crystal structure of RNase 1 bound to a nucleoside vanadate. That is not surprising, as RNase 1 has been crystallized in a complex with its inhibitor protein (Johnson et al. 2007) but not alone or in a complex with a small-molecule ligand. Accordingly, we sought insight about RNase 1 from molecular docking studies and MD simulations with the three dinucleotide substrates. The structures of UpA, ΨpA, and m¹ΨpA were optimized at the M06-2X/6-31+G(d,p) level of theory (Zhao and Truhlar 2008a,b) and docked into the active site of RNase A (Supplemental Fig. S9) and RNase 1 (Supplemental Fig. S10). MD simulations for each substrate were initiated from the enzyme substrate complexes resulting from the docking studies and were performed for 1500 nsec of simulation time. For each simulation, an average structure was generated using 7500 frames from the last 750 nsec. Overlays of the structures of the dinucleotide substrates bound to RNase 1 obtained from the MD simulations with the crystal structures of the nucleoside vanadates bound to RNase A are in accord (Fig. 4), suggesting that each substrate binds in a similar manner. We also performed MD simulations of the dinucleotide substrates bound to RNase A and observed highly similar

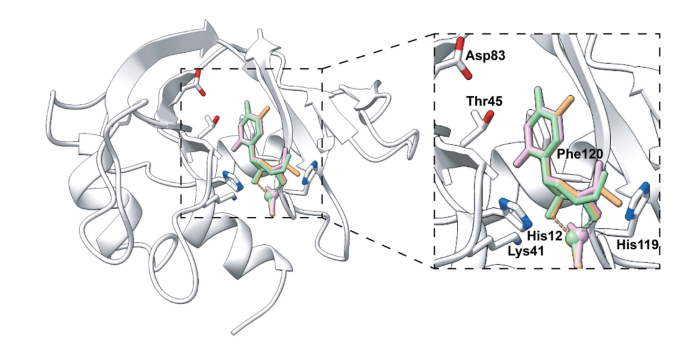


FIGURE 3. Overlay of the crystal structures of RNase A bound to U > v (pink), Ψ > v (green), and $m^1\Psi$ > v (orange). The protein representation (white) is from the Ψ > v crystal structure, and key residues for binding and catalysis are indicated explicitly. The nucleobase···Thr45 distances are RNase A·U > v: N³···Oγ¹, 2.72 Å; O²···N, 2.78 Å; RNase A·Ψ > v, N³···Oγ¹, 2.80 Å; O⁴···N, 2.83 Å; and RNase A·m¹Ψ > v, N³···Oγ¹, 2.81 Å; O⁴···N, 2.80 Å. Alignment was performed in Chimera X (Meng et al. 2023) using Matchmaker. The average ligand RMSD values are 0.509 Å and 0.439 Å for Ψ > v and $m^1\Psi$ > v with respect to U > v as calculated using only isologous heteroatoms and the coordinating vanadyl group.

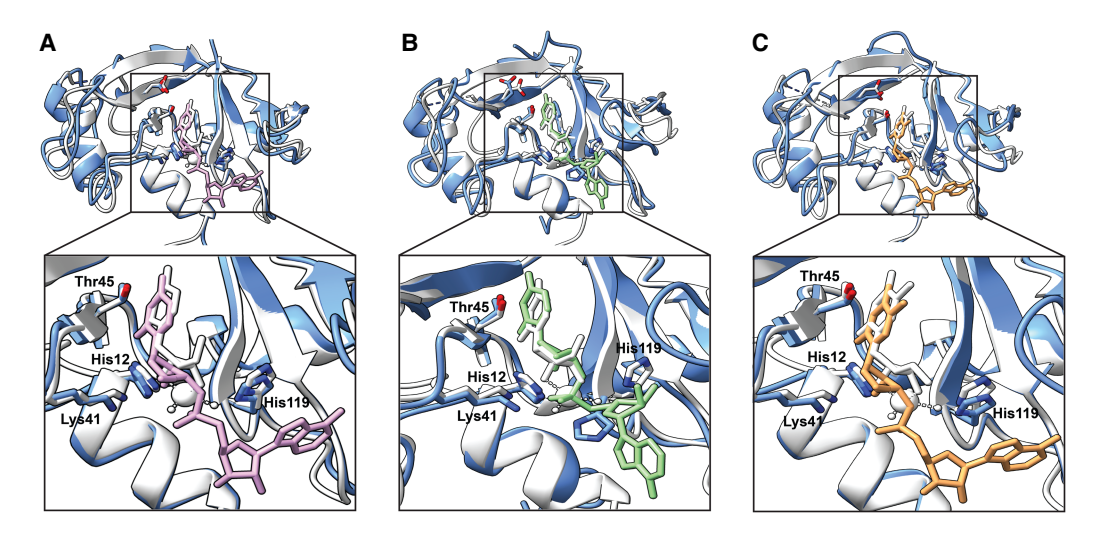


FIGURE 4. Overlay of UpA (A, pink), Ψ pA (B, green), and $M^1\Psi$ pA (C, orange) bound to RNase 1 (blue) obtained from the MD simulations with the respective crystal structures of U > v (A, white), $\Psi > v$ (B, white), and $M^1\Psi > v$ (C, white) bound to RNase A (white).

binding modes, consistent with the crystal structures (Supplemental Fig. S11).

A major challenge in computational chemistry is the development of methods to reliably predict the binding free energy (ΔG_{bind}) of a ligand to its receptor in a complex. Various methods have been developed, ranging from simple and fast scoring functions (Rajamani and Good 2007) to more rigorous but time-intensive approaches such as free energy perturbation (Michel and Essex 2010; Cournia et al. 2021). In between are the so-called end-point methods that use MD simulations, which take into account the dynamic nature of the bimolecular interaction, along with a molecular mechanics (MM) potential (Wang et al. 2019). MMGBSA (molecular mechanics-generalized Born surface area) is one of the widely used end-point methods for estimating the energetics of substrate binding (Kollman et al. 2000; Tsui and Case 2000; Rastelli et al. 2010; Ylilauri and Pentikäinen 2013; Mikulskis et al. 2014; Genheden and Ryde 2015). Here, binding free energies from the MD simulations were sampled from the last 750 nsec (using 7500 equally spaced frames).

The three dinucleotides share a similar binding pattern to RNase 1, with UpA generally showing the highest affinity and m¹ΨpA generally showing the lowest affinity in accord with the experimental data. The decomposition of binding energies into gas-phase energy contributions (electrostatic and van der Waals) and solvation free energy components (polar and nonpolar) shows that electrostatics dominate the overall binding of each substrate (Table 2). Similar nonpolar contributions imply that each substrate has a similar exposure to solvent and comparable hydrophobic properties. To further assess the energetic contributions of the important residues within the active site of RNase 1, we decomposed the binding energies on a per-residue basis. Once again, we observed similar contributions from four key residues, His12, Thr45, Asp83, and Phe120, to the overall binding free energies (Fig. 5). Lys41 makes a stronger contribution to binding the pseudouridines, and His119 makes a weaker contribution. The variability can be attributed to the proximity of Lys41 and His119 to the phosphoryl group and, for His119, the extent of aromatic donor-acceptor interactions with the adenine nucleobase.

TABLE 2. Decomposition of average MMGBSA binding energies (ΔG_{bind} , kcal/mol) of RNase 1 for dinucleotide substrates into gas-phase energy contributions ($\Delta E_{\text{van der Waals}}$ and $\Delta E_{\text{electrostatics}}$) and solvation free energy components (G_{polar} and G_{nonpolar})

m ¹ ΨpA
-45.75
-286.11
294.64
-5.59
-42.81

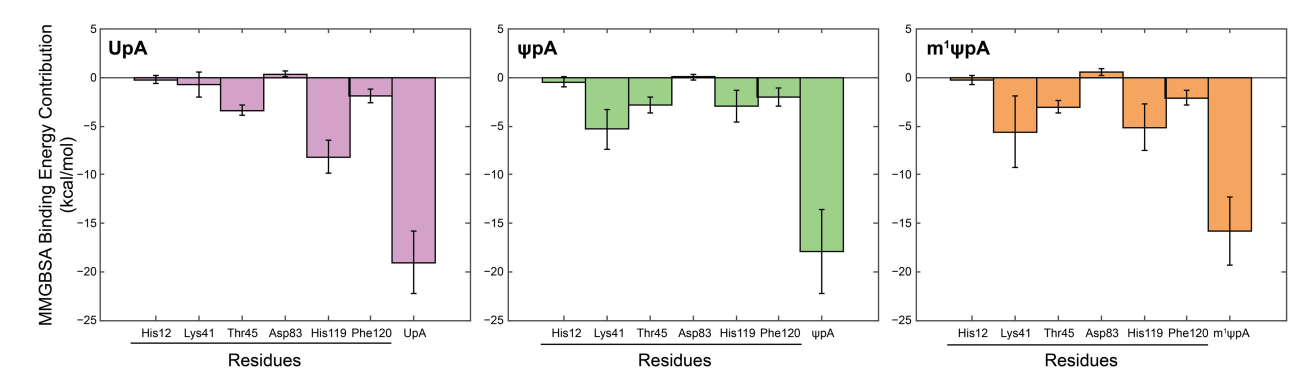


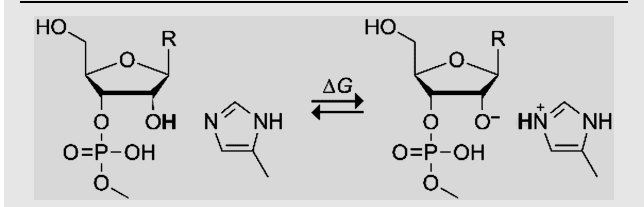
FIGURE 5. Average per-residue MMGBSA binding energy contributions of the key residues of RNase 1 to dinucleotide substrates. Values are the average \pm SD for each residue over 7500 frames.

Basis for the differential catalysis of UpA, Ψ pA, and m¹ Ψ pA cleavage

The diminished ability of the ptRNases to turn over the pseudouridine substrates was manifested in $k_{\rm cat}$ rather than $K_{\rm M}$ (Table 1). In accord, MD simulations of the binding of the three substrates to RNase 1 did not reveal differential interactions. Likewise, crystal structures of the three nucleoside vanadates bound to RNase A were indistinguishable. Having ruled out binding to the substrates or products as the primary contributor to differential kinetics, we focused on the transition states. Specifically, we wondered whether an unappreciated electronic effect could explain the lower $k_{\rm cat}$ and $k_{\rm cat}$ / $K_{\rm M}$ values for the pseudouridine substrates.

In uridine, the pyrimidine nucleobase is linked to the ribose by a β -N-glycosidic bond, whereas in the pseudouridines, that linkage is a β -C-glycosidic bond (Fig. 1). On the Pauling scale, the electronegativity of nitrogen (χ = 3.0) is greater than that of carbon (χ = 2.5) (Pauling 1939). Moreover, N^1 of uridine is conjugated to functional groups in the nucleobase (Fig. 1) that further increase its ability to

TABLE 3. Relative free energies for the deprotonation of the 2'-hydroxy group of nucleoside 3'-methylphosphates by 4-methylimidazole with respect to the sum of the reactant energies at infinite separation ([SMD-H₂O] M06-2X/6-31+G(d,p))



Uracil 18.4 Pseudouracil 21.3 N¹-methylpseudouracil 21.0	Nucleobase (R)	ΔG (kcal/mol)
	Uracil	18.4
N^1 -methylpseudouracil 21.0	Pseudouracil	21.3
	N ¹ -methylpseudouracil	21.0

withdraw electron density. We reasoned that the enhanced inductive effect of N^1 in uridine decreases the p K_a of its 2'-hydroxy group relative to that in pseudouridines. The deprotonation of that 2'-hydroxy group is necessary for cleavage by ptRNases (Findlay et al. 1961; Cuchillo et al. 2011), and a lower p K_a should decrease the energy of the transition state and thereby increase reactivity (Dantzman and Kiessling 1996).

To provide insight into the relative acidities of the 2'-hydroxy groups of the substrates, we modeled the first step in the catalysis of RNA cleavage. In that step, the imidazolyl group in His12 acts as a base that abstracts a proton from the 2'-hydroxy group (Jackson et al. 1994; Thompson and Raines 1994). In UpA, the p K_a of the uridylyl 2'-hydroxy group is 12.54 (Järvinen et al. 1991). We used density functional theory with the SMD solvation model to calculate the free energy change associated with a proton transfer between three nucleoside 3'-methylphosphates and 4methylimidazole. We selected this approach to circumvent issues with accurately predicting the solvation energy of a proton (Ho and Coote 2010; Prasad and Tantillo 2021). The resulting free energies suggest that the pK_a of the 2'-hydroxy group of uridine 3'-phosphate is lower than those of pseudouridine 3'-methylphosphate and N¹-methylpseudouridine 3'-methylphosphate, which are similar (Table 3).

We reasoned that the differential p K_a for uridine versus a pseudouridine would be manifested in their intrinsic reactivity. To test this hypothesis, we assessed the uncatalyzed cleavage of UpA and m¹ΨpA. At pH 6.0 and 25°C, the rate constant for the uncatalyzed cleavage of UpA is $k_{uncat} = 5 \times 10^{-9} \, {\rm sec}^{-1}$, which corresponds to $t_{1/2} = 4$ years (Thompson et al. 1995). To accelerate the time course, we chose to monitor the cleavage reactions at a higher pH (10.0) and temperature (90°C), using a buffer (2-(cyclohexylamino) ethanesulfonic acid [CHES]) with a p K_a of known temperature-dependence (Roy et al. 1997). We note that the p K_a of the N^3 -H imido group of uridine and N^1 -methylpseudouridine are similar (Jones et al. 2022), and both will be mostly unprotonated at pH 10.0.

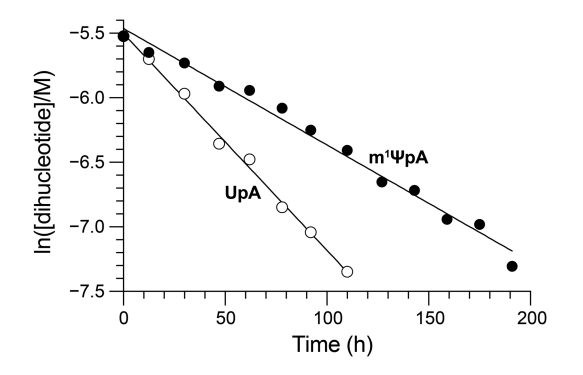


FIGURE 6. Nonenzymatic cleavage rate of UpA and $m^1\Psi pA$ in 0.10 M CHES–NaOH buffer, pH 10.0, containing NaCl (0.10 M) at 90°C as monitored with ^{31}P NMR spectroscopy.

We used ³¹P nuclear magnetic resonance (NMR) spectroscopy to monitor the nonenzymatic cleavage of UpA and m¹ΨpA (Supplemental Figs. S18, S19). We found that UpA ($k_{\rm uncat} = 4.7 \pm 0.1 \times 10^{-6} \ {\rm sec}^{-1}$; $t_{1/2} = 41 \ h$) is more vulnerable to spontaneous cleavage than is m¹ΨpA ($k_{\rm uncat} = 2.5 \pm 0.1 \times 10^{-6} \ {\rm sec}^{-1}$; $t_{1/2} = 77 \ h$) (Fig. 6). These experimental data are consistent with the inductive effect of the uracil nucleobase on the p $K_{\rm a}$ of the 2′-hydroxy group in uridine (Table 3) and with the higher $k_{\rm cat}$ and $k_{\rm cat}$ / $K_{\rm M}$ values for catalysis of UpA cleavage by ptRNases (Table 1).

DISCUSSION

ptRNases degrade RNA in a largely nonspecific manner, governed only by the requirement that cleavage of the P–O^{5"} bond occurs directly after a pyrimidine residue. We discovered that nucleotides containing Ψ and $m^1\Psi$ are accommodated in the active site of both RNase A and RNase 1 and allow for catalysis, though at a lower level than U. Additionally, we found that the binding of Ψ and $m^1\Psi$ occurs in a similar manner to that of U and obtained, to the extent of our knowledge, the first crystal structure of a protein bound to Ψ (Hoang and Ferré-D'Amaré 2001).

Catalysis by RNase 1 had not been examined previously with a dinucleotide substrate. ptRNases have multiple subsites that bind to phosphoryl groups in RNA substrates (Fisher et al. 1998; Nogués et al. 1998). With a tetranucleotide substrate (Supplemental Fig. S2), catalysis by RNase A is only fourfold more efficient than by RNase 1 under optimal conditions (Supplemental Table S1). This difference increases, however, to 33-fold with a dinucleotide substrate. Although RNase A and RNase 1 are homologous and share 68% of their amino acid residues, the two enzymes evolved in distinct niches and have different physiological roles (Eller et al. 2014). For example, RNase A could serve as an important scavenger of inorganic phosphate for ruminants (Barnard 1969), a role that benefits from the turnover of even the smallest RNA substrates.

Along these lines, we found that RNase A is more sensitive than RNase 1 to uracil modifications. This drop-off could be related to the more specific function of RNase A in the ruminant gut, where RNase A might have evolved to turn over RNA containing canonical nucleotides. Unlike RNase A, human RNase 1 can turn over a large diversity of RNA substrates, including double-stranded RNA (Lomax et al. 2017), the RNA strand of RNA:DNA hybrids (Potenza et al. 2006), and even poly(A), albeit at a low level (Sorrentino 1998). These enzymatic activities are consistent with RNase 1 being expressed at significant levels in many tissues and having functions that require a broader substrate scope that modulates the innate immune response, vascular homeostasis, and scavenging of extracellular RNA (Sorrentino 2010; Koczera et al. 2016; Garnett et al. 2019). Apparently, RNase 1 can accommodate pyrimidine variations better than RNase A. In living systems, RNA occurs in diverse sizes, structures, compositions, and sequences, and the trends reported here might be amplified or reduced, depending on the context as well as the biochemical environment.

Structurally, we observed little difference in the binding of the three phosphodiester product analogs to RNase A. Nor did MD simulations reveal significant overall differences in substrate binding to either RNase A or RNase 1. We calculated, however, that the differential glycosidic connectivity of the nucleobase in uridine and the pseudouridines alters the p K_a of the 2'-hydroxy group, decreasing the intrinsic reactivity of pseudouridine nucleotides. In accord, we found a lesser difference in the enzymatic turnover of UpA, Ψ pA, and m¹ Ψ pA at pH 7.5 than at pH 6.0. This discovery expands our fundamental understanding of the most abundant modified nucleoside in natural RNA and has implications for RNA biology. For example, we are intrigued by the possibility that a role of pseudouridine is to stabilize natural RNA structures with a relatively linear O2'...P-O5" alignment, which would otherwise be more vulnerable to spontaneous cleavage. Likewise, the chemical stability conferred by N¹-methylpseudouridine has evident benefits for the ongoing development of RNA-based vaccines and therapeutic agents.

MATERIALS AND METHODS

Production and purification of RNase 1

Human RNase 1 was produced in *E. coli* without its signal peptide and with an N-terminal methionine residue as described previously (Ressler et al. 2019), with minor modifications. The expression plasmid was transformed into BL21(DE3) cells. A starter culture (50 mL) was inoculated from a single colony and grown overnight at 37°C in TB containing ampicillin (200 μ g mL⁻¹) with constant shaking at 250 rpm. Cultures (1.0 L) were initiated at OD_{600 nm} = 0.05 from the starter culture and grown at 37°C in TB containing ampicillin (200 μ g mL⁻¹) with constant shaking at

250 rpm. Gene expression was induced with isopropyl-β-D-1-thiogalactopyranoside (IPTG) (final concentration: 1.0 mM) when the cultures reached OD_{600 nm} = 1.8–2.2 and were grown for an additional 3 h at 37°C. Cells were pelleted by centrifugation at 6000g for 15 min at 4°C, and cell pellets were stored at -80°C until resuspension and lysis.

Cell pellets containing RNase 1 were resuspended in 20 mM Tris-HCl buffer, pH 7.6, containing 10 mM EDTA (1 g of wet pellet per 10 mL of buffer). Cells were lysed at 19.0 kpsi at 4°C using a benchtop cell disruptor from Constant Systems. Inclusion bodies were isolated by centrifugation at 30,000g for 1.5 h at 4°C. The resultant inclusion bodies were resuspended in 20 mM Tris-HCl buffer, pH 8.0, containing guanidine-HCl (7 M), dithiothreitol (DTT) (0.10 M), and EDTA (10 mM) for 2 h at room temperature (4 mL of buffer per 1 L of expression culture). The solution was then diluted 10-fold with 20 mM acetic acid, and the insoluble material was removed by centrifugation at 16,500g for 30 min at 4°C. The clarified supernatant was dialyzed against 16 L of 20 mM acetic acid overnight at 4°C using a 3.5k MWCO bag. The dialysate was then subjected to centrifugation at 30,000g for 1 h at 4°C to remove additional insoluble material. To fold the RNase 1, the clarified supernatant was added dropwise with gentle stirring to 100 mM Tris-HCl buffer, pH 7.8, containing NaCl (0.10 M), reduced glutathione (1.0 mM), and oxidized glutathione (0.2 mM). This incubation was continued at 4°C without stirring for at least 2 days. The pH of the solution was then adjusted to 5.0 by adding 3 M sodium acetate buffer, pH 5.0, and the resulting solution was passed through a 0.45 µm filter. The sterilized solution was concentrated using an Amicon Stirred Cell concentrator from EMD Millipore with 10 kDa filters. Further purification was done with an ÅKTA pure FPLC system from Cytiva. Gel-filtration chromatography was performed with a Superdex HiLoad 26/600 75 pg gel filtration column and 50 mM sodium acetate buffer, pH 5.0, containing NaCl (0.10 M) and sodium azide (0.05% w/v). Fractions containing the ribonuclease were pooled and purified further by chromatography with a HiTrap SP cation-exchange column and 50 mM sodium acetate buffer, pH 5.0, containing a linear gradient of NaCl (0.35-0.70 M) over 35 column volumes. Fractions containing RNase 1 were pooled, concentrated, and buffer-exchanged into 50 mM Tris-HCl, pH 7.5, containing NaCl (50 mM) using an Amicon 15 mL 10 kDa MWCO spin concentrator. The identity of the protein was validated with QTOF mass spectrometry and SDS-PAGE. Aliquots were flash-frozen in $N_2(I)$ and stored at -70° C. Typically, ~2 mg of RNase 1 was obtained per liter of culture.

Kinetic measurements of dinucleotide cleavage

UpA, ΨpA, and m¹ΨpA were synthesized from their component nucleosides by using the phosphoramidite method (Scheme 1; Caruthers 2011). (For experimental details, see the Supplemental Material.) The cleavage of UpA, ΨpA, and m¹ΨpA by RNase A and RNase 1 was assayed by monitoring the change in absorbance of the substrate near 280 nm (Witzel and Barnard 1962). (Note: A coupled assay using adenosine deaminase [Ipata and Felicioli 1968] was not feasible because commercial sources of adenosine deaminase catalyze the hydrolysis of adenine nucleobase in the substrate as well as the product.) For each substrate, the exact wavelength was chosen by analyzing UV spectra before

and after cleavage and choosing the wavelength with the maximal difference (Supplemental Table S2; Supplemental Fig. S4). Assays were performed with a Spark plate reader from Tecan in 96-well half-area UV star microplates with a final volume of 50 μL. For RNase A, reactions were performed in 0.10 M DEPC-treated OVS-free MES-NaOH buffer, pH 6.0, containing NaCl (0.10 M), which is the pH at which RNase A is most active (Lomax et al. 2017). RNase 1 reactions were performed in 0.10 M Tris-HCl buffer, pH 7.5, containing NaCl (0.10 M), which is the pH at which RNase 1 is most active (Lomax et al. 2017). This buffer was made from DEPC-treated water and a DEPC-treated stock solution of NaCl (1.0 M). Assays were conducted at 25°C with a substrate concentration of 50–1000 µM. Due to the lack of sensitivity of this assay, the concentration of ribonuclease in each reaction was optimized to have a high dynamic range while maintaining linearity in the initial region. For RNase A, concentrations of 1, 4, and 10 nM were used; for RNase 1, concentrations of 10, 20, and 20 nM were used for UpA, ΨpA, and m¹ΨpA, respectively. To obtain the baseline absorbance of a well and ensure no contamination from exogenous ribonucleases, 25 µL of a 2× solution of substrate in the appropriate buffer was added to each well, and the absorbance was measured over 2 min. Then, a 2× solution of RNase A or RNase 1 was added to the substrate, and the absorbance was measured over 20 min. To obtain the absorbance of fully cleaved substrate, 25 µL of a solution of RNase A $(4 \mu M)$ was added to 25 μL of the 2× solution of substrate in a separate well, and the absorbance was measured over 10 min. The measurements were performed at wavelengths optimized for each enzyme-substrate pair as listed in Supplemental Table S2. Initial rates were plotted against substrate concentration and fitted to the Michaelis-Menten equation to determine values of k_{cat} and K_{M} . (See the Supplemental Material for additional details.)

For the pH-dependent experiments, assays were performed as above, except in the buffer corresponding to the desired pH. Values of $k_{\rm cat}/K_{\rm M}$ were determined by performing linear fits in regions of low [S]. (See the Supplemental Material for additional details.)

For the nonenzymatic cleavage experiments, a solution of UpA (4.0 mM) and a solution of $m^{1}\Psi pA$ (4.0 mM) were prepared in 0.10 M CHES-NaOH buffer, pH 10.0, containing NaCl (0.10 M) under ribonuclease-free conditions. The solutions were added to NMR tubes. Sealed capillaries containing phenylphosphonic acid (50 mM) in D_2O containing NaCl (0.10 M) were placed into the tubes as a reference. Both tubes were kept under identical conditions at all times. The tubes were incubated at 90°C for the specified amount of time. Before acquiring ³¹P NMR spectra, the samples were cooled to room temperature. Undecoupled ³¹P NMR spectra (scans: 64, relaxation delay: 12 sec, center: 10 ppm, spectral width: 50 ppm) were obtained at each time point. To calculate the concentration of UpA or m¹ΨpA at a particular time point, the integral of the signal from UpA (-0.69 ppm) or $m^{1}\Psi pA$ (-0.48 ppm) was normalized to the integral of the signal from phenylphosphonic acid (15.99 ppm). Signals from each 2',3'-cyclic phosphate (~20 ppm) and 2'- and 3'-phosphates (~3-4 ppm) appeared during the time course of the reaction (Supplemental Figs. \$18, \$19). Integrals of sufficient accuracy could be obtained only to a dinucleotide concentration of ≥0.8 mM. Spectra were processed with MestReNova software (version 14.1.1-24571) using automatic baseline and phase correction tools. Rate constants were obtained with linear least-squares regression analyses using Origin 2021 software (version: 9.8.0.200).

Crystallization of RNase A with nucleoside vanadates

RNase A was crystallized as described previously with some minor modifications. RNase A was dissolved in water to a 20 mg/ mL stock concentration. Crystals were initially grown via the hanging drop method using a reservoir of 20 mM sodium citrate buffer, pH 5.5, containing 20% PEG 4000 (20% w/v) and a drop that was a 1:1 solution of reservoir:RNase A stock solution. The drops were incubated at 16°C. Crystals appeared in \sim 7–10 days. Additional crystals were obtained by seeding small or fragmented crystals from the initial growth via a seeding tool into various solutions via the hanging drop method. In general, the seeded crystals grew larger at 16°C with reservoir solutions of 20 mM sodium citrate buffer, pH 5.5, or 50 mM imidazole-HCl buffer, pH 5.5, containing PEG 4000 (20%-25% w/v) and tert-butanol (0%-10% w/v) and drops that were 1:1 solutions of reservoir: RNase A stock solution. Seeded crystals grew in ~3-7 days. After crystals formed, they were stable at 16°C-25°C for at least a month in the dark. The highest quality crystals grew in 20 mM sodium citrate buffer, pH 5.5, containing PEG 4000 (25% w/v) and were used for subsequent soaking experiments with $\Psi > v$ and $m^1\Psi > v$. For the U > v experiments, crystals were formed via seeding into 50 mM imidazole-HCl, pH 5.5, containing PEG 4000 (20% w/v).

To obtain ligand-bound structures, nucleoside vanadates were soaked into RNase A crystals. The nucleoside vanadate solutions were prepared as described previously with minor modifications (Ladner et al. 1997). Briefly, uridine or a pseudouridine (45 mg) was mixed with ammonium vanadate (NH₄VO₃; 105 mg) in 6.1 mL of 50 mM imidazole-HCl buffer, pH 5.2, and the resulting solution was heated to 60°C for 20 min on a hotplate with stirring. The resulting solutions were yellow and, after cooling to room temperature, constituted the stock solution for each ligand. For U > v, crystals were transferred into hanging drops containing a 2:1 mixture of U > v stock solution:25 mM imidazole-HCl buffer, pH 5.5, containing PEG 4000 (30% w/v) over a reservoir of the same composition. These hanging drops were incubated at room temperature for 2 days. Prior to freezing and data collection, the crystals were dipped into cryoprotectant conditions, which were 16.7 mM imidazole-HCl buffer, pH 5.5, containing U > v stock solution (33% v/v), PEG 4000 (30% w/v), and glycerol (5% v/v), before they were flash-cooled in a stream of cryogenic $N_2(g)$ for data collection. For $\Psi > v$, crystals were transferred into hanging drops of 16.7 mM imidazole-HCl buffer, pH 5.5, containing $\Psi > v$ stock solution (33% v/v), PEG 4000 (30% w/v), and glycerol (5% v/v). These hanging drops were incubated at room temperature for 2 days before being directly frozen in cryogenic $N_2(g)$ and then data collection. For $m^1\Psi$ > v, crystals were transferred into hanging drops of 16.7 mM imidazole-HCl buffer, pH 5.5, containing $m^{1}\Psi > v$ stock solution (33% v/v), PEG 4000 (30% w/v), and glycerol (5% v/v). These hanging drops were incubated at room temperature for 1 day before being directly frozen in cryogenic N₂(g) and subsequent data collection.

Data collection, processing, and structural determination

Data were collected on a Rigaku Micromax-007 rotating anode with Osmic VariMax-HF mirrors and a Rigaku Saturn 944 detector. The obtained data were processed with XDS (Kabsch 2010). Phaser (McCoy et al. 2007), as implemented in PHENIX (Liebschner et al. 2019), was used to solve the structures by molecular replacement, using the protein coordinates from the structure of RNase A in a complex with cytidine 3'-phosphate (PDB entry 5ogh [Prats-Ejarque et al. 2019]). Ligand structures were modeled and optimized with Gaussian 16 at the M06-2X/ $\,$ 6-31 + G(d,p) level (Zhao and Truhlar 2008a,b; Frisch et al. 2016) using restraints conforming to the configuration of the vanadyl group in the structure of RNase A in complex with U > v (PDB entry 1ruv [Ladner et al. 1997]). Structures were refined using PHENIX (Liebschner et al. 2019) with manual fitting in COOT (Emsley et al. 2010) and geometry improvement with Rosetta (DiMaio et al. 2013). Data and refinement statistics are listed in Supplemental Tables S4-S7.

Molecular docking

The structures of UpA, Ψ pA, and m¹ Ψ pA were optimized at the M06-2X/6-31 + G(d,p) level of theory using Gaussian 16 (Zhao and Truhlar 2008a,b; Frisch et al. 2016) and docked into the active site of RNase A and RNase 1 using AutoDock Vina (Trott and Olson 2010). During docking, the side chains of catalytic residues His12, His119, and Lys41 were treated as flexible, while the rest of the enzyme was treated as rigid. The resulting docked poses were scored, and poses were selected in which (1) the pyrimidine and Thr45, (2) the 2' hydroxy group and His12, (3) the phosphoryl group and Lys41, and (4) the 5"-oxygen and His119 were within the interaction distances (Supplemental Figs. S9, S10).

Molecular dynamics simulations setup

MD simulations were based on the complexes that resulted from the docking of UpA, Ψ pA, and $m^1\Psi$ pA into the active site of RNase A and RNase 1. The structure of RNase A was from PDB entry 1ruv (Ladner et al. 1997). The protonation states of RNase A residues were adjusted to those at pH 6.0. The structure of RNase 1 was based on chain X of PDB entry 2q4g (Johnson et al. 2007). Missing residues (i.e., the N-terminal lysine and C-terminal threonine) were modeled with MODELER software (Webb and Sali 2016). The protonation states of RNase 1 residues were adjusted to those at pH 7.5.

Molecular dynamics simulation protocol

MD simulations were performed on cuda-enabled gpus of particle mesh Ewald molecular dynamics (pmemd) in Amber 2022 (Case et al. 2023). We used the ff14SB and GAFF parameter sets for the protein and ligands, respectively (Wang et al. 2004; Maier et al. 2015). We also performed the simulations using the RNA force field OL3 (Zgarbova et al. 2011) and modrna08 (Aduri et al. 2007) for canonical and modified dinucleotide ligands, respectively (Supplemental Fig. S12). Restrained electrostatic potential charges (RESPs) were calculated with the R.E.D.

server (Bayly et al. 1993; Vanquelef et al. 2011). Each system was solvated in the TIP3P water model and neutralized in 0.10 M NaCl (Jorgensen et al. 1983). Each system was minimized and heated to 300 K using Langevin dynamics with a collisional frequency of 1 psec in the NVT ensemble over 100 psec with harmonic restraints of 10.0 kcal $\text{mol}^{-1} \text{ Å}^{-2}$ on protein and ligand. Further equilibration was performed in the NPT ensemble using isotropic position scaling and a pressure relaxation time of 2 psec at 300 K with harmonic restraints on the protein and ligand starting at 5.0 kcal mol⁻¹ $Å^{-2}$ and lifted slowly, giving a total of 12 nsec of restrained equilibration and 20 nsec of unrestrained equilibration time. The nonbonded cutoff was 9 Å. Each system was subjected to a 1500 nsec production run in the NPT ensemble using time steps of 2 fsec with Langevin dynamics and a Monte Carlo barostat at 300 K. The long-range electrostatic interactions were calculated using the particle mesh Ewald (PME) method.

Analysis protocols for molecular dynamics simulations

The binding free energies ($\Delta G_{\rm bind}$ in kcal/mol) were computed by using the molecular mechanics-generalized Born surface area (MMGBSA) method implemented in Amber 2022 using the last 750 nsec (using 7500 equally spaced simulation frames) and decomposed on a per-residue basis (Kollman et al. 2000; Tsui and Case 2000; Rastelli et al. 2010; Ylilauri and Pentikäinen 2013; Mikulskis et al. 2014; Genheden and Ryde 2015).

In the MMGBSA method, the free energy for binding is expressed as:

$$\Delta G_{bind} = G_{complex} - G_{protein} - G_{ligand},$$

where ΔG_{bind} is the binding free energy and $\Delta G_{\text{complex}}$ $\Delta G_{\text{protein}}$, and ΔG_{ligand} are the free energies of complex, protein, and ligand, respectively. ΔG_{bind} can be decomposed into

$$\Delta G_{bind} \!=\! \Delta E_{bnd} \! +\! \Delta E_{electrostatic} \! +\! \Delta E_{van\;der\;Waals} \! +\! \Delta G_{pol} \! +\! \Delta G_{np} \! -\! T \Delta S,$$

where the first three terms are MM energy components in gas phase from bonded (bond, angle, dihedral), electrostatic, and van der Waals interactions. $\Delta G_{\rm pol}$ is the polar contribution to the solvation free energy, which can be obtained by using the generalized Born (GB) model. The nonpolar contribution to the solvation free energy, $\Delta G_{\rm np}$, is estimated using the solvent-accessible surface area (SASA). Finally, $T\Delta S$ is the change in conformational entropy, which is often neglected when ranking binding free energies of similar ligands (Gohlke and Case 2004; Zhou and Madura 2004). In this study, the binding free energies were calculated using the single trajectory approach, resulting in the cancellation of bonded energy terms, and the entropy contribution was omitted to reduce computational cost. The GB calculations were performed using parameters developed previously (igb = 5 [α = 1.0, β = 0.8, γ = 4.85]) (Onufriev et al. 2004).

An average structure from each simulation was generated by *k*-means cluster analysis, and root mean square deviation (RMSD) analysis was performed to assess the stabilization of the protein structure (Supplemental Figs. S13–S15), using the CPPTRAJ module implemented in AmberTools23 (Roe and Cheatham 2013; Case et al. 2023). Likewise, a root mean square fluctuation (RMSF) analysis was performed to assess residue mobility (Supplemental Figs. S16, S17).

Quantum chemistry calculations for relative acidity predictions

Density functional theory calculations were performed using Gaussian 16 (Frisch et al. 2016) to provide insight into the relative acidity of the 2'-hydroxy groups of the substrates. The free energy that accompanies a proton transfer between three nucleoside 3'-methylphosphates and 4-methylimidazole was calculated at the [SMD-H₂O] M06-2X/6-31 + G(d,p) level of theory (Zhao and Truhlar 2008a,b).

SUPPLEMENTAL MATERIAL

Supplemental material is available for this article.

ACKNOWLEDGMENTS

We thank Alia A. Kassim for help in determining the extinction coefficients for UpA, ΨpA, and m¹ΨpA. C.S.G. was supported by a National Defense Science and Engineering Graduate Fellowship sponsored by the Air Force Research Laboratory. B.S. was supported by a Walter Benjamin fellowship from the Deutsche Forschungsgemeinschaft. J.A.P. was supported by a Studienstiftung des Deutschen Volkes fellowship. This work was supported by grant R01 CA073808 (National Institutes of Health) and used the MIT Structural Biology Core Facility and computational resources through allocation BIO230178 from the Advanced Cyberinfrastructure Coordination Ecosystem: Services & Support (ACCESS) program, which was supported by grants 2137603, 2138259, 2138286, 2138296, and 2138307 (National Science Foundation).

Received June 1, 2025; accepted July 28, 2025.

REFERENCES

Aduri R, Psciuk BT, Saro P, Taniga H, Schlegel HB, SantaLucia J. 2007. AMBER force field parameters for the naturally occurring modified nucleosides in RNA. *J Chem Theory Comput* **3:** 1464–1475. doi:10.1021/ct600329w

Anderson BR, Muramatsu H, Nallagatla SR, Bevilacqua PC, Sansing LH, Weissman D, Karikó K. 2010. Incorporation of pseudouridine into mRNA enhances translation by diminishing PKR activation. *Nucleic Acids Res* 38: 5884–5892. doi:10.1093/nar/gkq347

Anderson BR, Muramatsu H, Jha BK, Silverman RH, Weissman D, Karikó K. 2011. Nucleoside modifications in RNA limit activation of 2'-5'-oligoadenylate synthetase and increase resistance to cleavage by RNase L. *Nucleic Acids Res* **39:** 9329–9338. doi:10.1093/nar/gkr586

Andries O, McCafferty S, De Smedt SC, Weiss R, Sanders NN, Kitada T. 2015. N¹-Methylpseudouridine-incorporated mRNA outperforms pseudouridine-incorporated mRNA by providing enhanced protein expression and reduced immunogenicity in mammalian cell lines and mice. *J Control Release* **217**: 337–344. doi:10.1016/j.jconrel.2015.08.051

Barnard EA. 1969. Biological function of pancreatic ribonuclease. *Nature* **221**: 340–344. doi:10.1038/221340a0

Bayly CI, Cieplak P, Cornell W, Kollman PA. 1993. A well-behaved electrostatic potential based method using charge restraints for

- deriving atomic charges: the RESP model. *J Phys Chem A* **97:** 10269–10280. doi:10.1021/j100142a004
- Carlile TM, Rojas-Duran MF, Zinshteyn B, Shin H, Bartoli KM, Gilbert WV. 2014. Pseudouridine profiling reveals regulated mRNA pseudouridylation in yeast and human cells. *Nature* 515: 143–146. doi:10.1038/nature13802
- Caruthers MH. 2011. A brief review of DNA and RNA chemical synthesis. *Biochem Soc Trans* **39:** 575–580. doi:10.1042/BST0390575
- Case DA, Aktulga HM, Belfon K, Cerutti DS, Cisneros GA, Cruzeiro VWD, Forouzesh N, Giese TJ, Götz AW, Gohlke H, et al. 2023. AmberTools. J Chem Inf Model 63: 6183–6191. doi:10.1021/acs.jcim.3c01153
- Cerneckis J, Cui Q, He C, Yi C, Shi Y. 2022. Decoding pseudouridine: an emerging target for therapeutic development. *Trends Pharmacol Sci* **43:** 522–535. doi:10.1016/j.tips.2022.03.008
- Charette M, Gray MW. 2000. Pseudouridine in RNA: What, where, how, and why. *IUBMB Life* **49:** 341–351. doi:10.1080/ 152165400410182
- Chen Y, Lin J, Zhao Y, Ma X, Yi H. 2021. Toll-like receptor 3 (TLR3) regulation mechanisms and roles in antiviral innate immune responses. *J Zhejiang Univ Sci B* **22:** 609–632. doi:10.1631/jzus.B2000808
- Cohn WE, Volkin E. 1951. Nucleoside-5'-phosphates from ribonucleic acid. *Nature* **167:** 483–484. doi:10.1038/167483a0
- Coumia Z, Chipot C, Roux B, York DM, Sherman W. 2021. Free energy methods in drug discovery—Introduction. In Free energy methods in drug discovery: current state and future directions, Vol. 1397, pp. 1–38. American Chemical Society, Washington, DC.
- Cuchillo CM, Parés X, Guasch A, Barman T, Travers F, Nogués MV. 1993. The role of 2',3'-cyclic phosphodiesters in the bovine pancreatic ribonuclease A catalysed cleavage of RNA: intermediates or products? *FEBS Lett* **333:** 207–210. doi:10.1016/0014-5793 (93)80654-D
- Cuchillo CM, Nogués MV, Raines RT. 2011. Bovine pancreatic ribonuclease: fifty years of the first enzymatic reaction mechanism. *Biochemistry* **50**: 7835–7841. doi:10.1021/bi201075b
- D'Alessio G, Riordan JF. 1997. Ribonucleases: structures and functions. Academic Press, New York, NY.
- Damase TR, Sukhovershin R, Boada C, Taraballi F, Pettigrew RI, Cooke JP. 2021. The limitless future of RNA therapeutics. Front Bioeng Biotechnol 9: 628137. doi:10.3389/fbioe.2021.628137
- Dantzman CL, Kiessling LL. 1996. Reactivity of a 2'-thio nucleotide analog. J Am Chem Soc 118: 11715–11719. doi:10.1021/ja962265c
- delCardayré SB, Raines RT. 1994. Structural determinants of enzymatic processivity. *Biochemistry* 33: 6031–6037. doi:10.1021/bi00186a001
- delCardayré SB, Raines RT. 1995. A residue to residue hydrogen bond mediates the nucleotide specificity of ribonuclease A. *J Mol Biol* **252:** 328–336. doi:10.1006/jmbi.1995.0500
- Demongeot J, Fougère C. 2022. mRNA COVID-19 vaccines—facts and hypotheses on fragmentation and encapsulation. *Vaccine* **11:** 40. doi:10.3390/vaccines11010040
- DiMaio F, Echols N, Headd JJ, Terwilliger TC, Adams PD, Baker D. 2013. Improved low-resolution crystallographic refinement with Phenix and Rosetta. Nat Methods 10: 1102–1104. doi:10.1038/ nmeth.2648
- Eller CH, Lomax JE, Raines RT. 2014. Bovine brain ribonuclease is the functional homolog of human ribonuclease 1. *J Biol Chem* **289**: 25996–26006. doi:10.1074/jbc.M114.566166
- Emsley P, Lohkamp B, Scott WG, Cowtan K. 2010. Features and development of Coot. Acta Crystallogr D 66: 486–501. doi:10.1107/S0907444910007493
- Findlay D, Herries DG, Mathias AP, Rabin BR, Ross CA. 1961. The active site and mechanism of action of bovine pancreatic ribonuclease. *Nature* **190:** 781–784. doi:10.1038/190781a0

- Fisher BM, Grilley JE, Raines RT. 1998. A new remote subsite in ribonuclease A. *J Biol Chem* **273**: 34134–34138. doi:10.1074/jbc.273 .51.34134
- Fontecilla-Camps JC, de Llorens R, le Du MH, Cuchillo CM. 1994. Crystal structure of ribonuclease A·d(ApTpApApG) complex. *J Biol Chem* **269**: 21526–21531. doi:10.1016/S0021-9258(17) 31836-7
- Frisch MJ, Trucks GW, Schlegel HB, Scuseria GE, Robb MA, Cheeseman JR, Scalmani G, Barone V, Petersson GA, Nakatsuji H, et al. 2016. *Gaussian 16 Rev. C.01*. Wallingford, CT.
- Garnett ER, Raines RT. 2022. Emerging biological functions of ribonuclease 1 and angiogenin. *Crit Rev Biochem Mol Biol* **57:** 244–260. doi:10.1080/10409238.2021.2004577
- Garnett ER, Lomax JE, Mohammed BM, Gailani D, Sheehan JP, Raines RT. 2019. Phenotype of ribonuclease 1 deficiency in mice. RNA 25: 921–934. doi:10.1261/rna.070433.119
- Genheden S, Ryde U. 2015. The MM/PBSA and MM/GBSA methods to estimate ligand-binding affinities. *Expert Opin Drug Discov* **10:** 449–461. doi:10.1517/17460441.2015.1032936
- Gohlke H, Case DA. 2004. Converging free energy estimates: MM-PB (GB)SA studies on the protein–protein complex Ras–Raf. *J Comput Chem* **25:** 238–250. doi:10.1002/jcc.10379
- Green MR, Sambrook J. 2019. How to win the battle with RNase. *Cold Spring Harb Protoc* **2019:** 95–98. doi:10.1101/pdb.top101857
- Guzzi N, Cieśla M, Ngoc PCT, Lang S, Arora S, Dimitriou M, Pimková K, Sommarin MN, Munita R, Lubas M. 2018. Pseudouridylation of tRNA-derived fragments steers translational control in stem cells. Cell 173: 1204–1216.e1226. doi:10.1016/j .cell.2018.03.008
- Ho J, Coote ML. 2010. A universal approach for continuum solvent pK_a calculations: Are we there yet? Theor Chem Acc **125**: 3–21. doi:10.1007/s00214-009-0667-0
- Hoang C, Ferré-D'Amaré AR. 2001. Cocrystal structure of a tRNA Ψ55 pseudouridine synthase: nucleotide flipping by an RNA-modifying enzyme. Cell 107: 929–939. doi:10.1016/S0092-8674(01)00618-3
- Hudson GA, Bloomingdale RJ, Znosko BM. 2013. Thermodynamic contribution and nearest-neighbor parameters of pseudouridineadenosine base pairs in oligoribonucleotides. RNA 19: 1474– 1482. doi:10.1261/ma.039610.113
- Ipata PL, Felicioli RA. 1968. A spectrophotometric assay for ribonuclease activity using cytidylyl-(3',5')-adenosine and uridylyl-(3',5')adenosine as substrates. FEBS Lett 1: 29–31. doi:10.1016/0014-5793(68)80010-9
- Islam MS, Bandyra KJ, Chao Y, Vogel J, Luisi BF. 2021. Impact of pseudouridylation, substrate fold, and degradosome organization on the endonuclease activity of RNase E. RNA 27: 1339–1352. doi:10.1261/rna.078840.121
- Jackson DY, Burnier J, Quan C, Stanley M, Tom J, Wells JA. 1994. A designed peptide ligase for total synthesis of ribonuclease A with unnatural catalytic residues. *Science* **266**: 243–247. doi:10 .1126/science.7939659
- Järvinen P, Oivanen M, Lönnberg H. 1991. Interconversion and phosphoester hydrolysis of 2',5'- and 3',5'-dinucleoside monophosphates: kinetics and mechanisms. *J Org Chem* **56:** 5396–5401. doi:10.1021/jo00018a037
- Jiang J, Kharel DN, Chow CS. 2015. Modulation of conformational changes in helix 69 mutants by pseudouridine modifications. *Biophys Chem* **200**: 48–55. doi:10.1016/j.bpc.2015.03.001
- Johnson RJ, McCoy JG, Bingman CA, Phillips GN Jr, Raines RT. 2007. Inhibition of human pancreatic ribonuclease by the human ribonuclease inhibitor protein. *J Mol Biol* 368: 434–449. doi:10.1016/j.jmb.2007.02.005
- Jones EL, Mlotkowski AJ, Hebert SP, Schlegel HB, Chow CS. 2022. Calculations of pK_a values for a series of naturally occurring

- modified nucleobases. *J Phys Chem A* **126:** 1518–1529. doi:10.1021/acs.jpca.1c10905
- Jorgensen WL, Chandrasekhar J, Madura JD, Impey RW, Klein ML. 1983. Comparison of simple potential functions for simulating liquid water. J Chem Phys 79: 926–935. doi:10.1063/1.445869
- Kabsch W. 2010. XDS. Acta Crystallogr D **66:** 125–132. doi:10.1107/ S0907444909047337
- Karijolich J, Yi C, Yu Y-T. 2015. Transcriptome-wide dynamics of RNA pseudouridylation. Nat Rev Mol Cell Biol 16: 581–585. doi:10 .1038/nrm4040
- Karikó K, Ni H, Capodici J, Lamphier M, Weissman D. 2004. mRNA is an endogenous ligand for Toll-like receptor 3. *J Biol Chem* **279**: 12542–12550. doi:10.1074/jbc.M310175200
- Karikó K, Buckstein M, Ni H, Weissman D. 2005. Suppression of RNA recognition by Toll-like receptors: the impact of nucleoside modification and the evolutionary origin of RNA. *Immunity* 23: 165– 175. doi:10.1016/j.immuni.2005.06.008
- Karikó K, Muramatsu H, Welsh FA, Ludwig J, Kato H, Akira S, Weissman D. 2008. Incorporation of pseudouridine into mRNA yields superior nonimmunogenic vector with increased translational capacity and biological stability. Mol Ther 16: 1833–1840. doi:10.1038/mt.2008.200
- Karikó K, Muramatsu H, Ludwig J, Weissman D. 2011. Generating the optimal mRNA for therapy: HPLC purification eliminates immune activation and improves translation of nucleoside-modified, protein-encoding mRNA. *Nucleic Acids Res* 39: e142. doi:10.1093/ nar/gkr695
- Kelemen BR, Schultz LW, Sweeney RY, Raines RT. 2000. Excavating an active site: the nucleobase specificity of ribonuclease A. Biochemistry 39: 14487–14494. doi:10.1021/bi001862f
- Kierzek E, Malgowska M, Lisowiec J, Turner DH, Gdaniec Z, Kierzek R. 2013. The contribution of pseudouridine to stabilities and structure of RNAs. *Nucleic Acids Res* 42: 3492–3501. doi:10.1093/nar/gkt1330
- Koczera P, Martin L, Marx G, Schuerholz T. 2016. The ribonuclease a superfamily in humans: canonical RNases as the buttress of innate immunity. Int J Mol Sci 17: 1278. doi:10.3390/ijms17081278
- Kollman PA, Massova I, Reyes C, Kuhn B, Huo S, Chong L, Lee M, Lee T, Duan Y, Wang W, et al. 2000. Calculating structures and free energies of complex molecules: Combining molecular mechanics and continuum models. Acc Chem Res 33: 889–897. doi:10.1021/ar000033j
- Krammer F, Palese P. 2024. Profile of Katalin Karikó and Drew Weissman: 2023 Nobel laureates in Physiology or Medicine. Proc Natl Acad Sci 121: e2400423121. doi:10.1073/pnas.2400423121
- Krauss M, Basch H. 1992. Is the vanadate anion an analogue of the transition state of RNase A? *J Am Chem Soc* **114:** 3630–3634. doi:10.1021/ja00036a008
- Ladner JE, Wladkowski BD, Anders Svensson L, Sjolin L, Gilliland GL. 1997. X-ray structure of a ribonuclease A-uridine vanadate complex at 1.3 Å resolution. Acta Crystallogr D Biol Crystallogr 53: 290–301. doi:10.1107/S090744499601582X
- Li X, Zhu P, Ma S, Song J, Bai J, Sun F, Yi C. 2015. Chemical pulldown reveals dynamic pseudouridylation of the mammalian transcriptome. *Nat Chem Biol* **11:** 592–597. doi:10.1038/nchembio.1836
- Liebschner D, Afonine PV, Baker ML, Bunkóczi G, Chen VB, Croll TI, Hintze B, Hung LW, Jain S, McCoy AJ, et al. 2019. Macromolecular structure determination using X-rays, neutrons and electrons: recent developments in Phenix. Acta Crystallogr D 75: 861–877. doi:10.1107/S2059798319011471
- Lindquist RN, Lynn JL Jr, Lienhard GE. 1973. Possible transition-state analogs for ribonuclease. The complexes of uridine with oxovanadium(IV) ion and vanadium(V) ion. *J Am Chem Soc* **95**: 8762–8768. doi:10.1021/ja00807a043

- Lomax JE, Eller CH, Raines RT. 2017. Comparative functional analysis of ribonuclease 1 homologs: molecular insights into evolving vertebrate physiology. *Biochem J* **474:** 2219. doi:10.1042/BCJ20170173
- Maier JA, Martinez C, Kasavajhala K, Wickstrom L, Hauser KE, Simmerling C. 2015. ff14SB: improving the accuracy of protein side chain and backbone parameters from ff99SB. J Chem Theory Comput 11: 3696–3713. doi:10.1021/acs.jctc.5b00255
- Marshall GR, Feng JA, Kuster DJ. 2008. Back to the future: ribonuclease A. *Biopolymers* **90:** 259–277. doi:10.1002/bip.20845
- McCoy AJ, Grosse-Kunstleve RW, Adams PD, Winn MD, Storoni LC, Read RJ. 2007. Phaser crystallographic software. J Appl Crystallogr 40: 658–674. doi:10.1107/S0021889807021206
- Meng EC, Goddard TD, Pettersen EF, Couch GS, Pearson ZJ, Morris JH, Ferrin TE. 2023. UCSF ChimeraX: tools for structure building and analysis. *Protein Sci* 32: e4792. doi:10.1002/pro .4792
- Messmore JM, Raines RT. 2000a. Decavanadate inhibits catalysis by ribonuclease A. Arch Biochem Biophys **381:** 25–30. doi:10.1006/abbi.2000.1951
- Messmore JM, Raines RT. 2000b. Pentavalent organo-vanadates as transition state analogues for phosphoryl transfer reactions. *J Am Chem Soc* **122**: 9911–9916. doi:10.1021/ja0021058
- Michel J, Essex JW. 2010. Prediction of protein-ligand binding affinity by free energy simulations: assumptions, pitfalls and expectations. *J Comput Aided Mol Des* **24**: 639–658. doi:10.1007/s10822-010-9363-3
- Mikulskis P, Genheden S, Ryde U. 2014. Effect of explicit water molecules on ligand-binding affinities calculated with the MM/GBSA approach. *J Mol Model* **20:** 2273. doi:10.1007/s00894-014-2273-x
- Morais P, Adachi H, Yu YT. 2021. The critical contribution of pseudouridine to mRNA COVID-19 vaccines. Front Cell Dev Biol 9: 789427. doi:10.3389/fcell.2021.789427
- Motorin Y, Helm M. 2010. tRNA stabilization by modified nucleotides. *Biochemistry* **49:** 4934–4944. doi:10.1021/bi100408z
- Nance KD, Meier JL. 2021. Modifications in an emergency: the role of N¹-methylpseudouridine in COVID-19 vaccines. *ACS Cent Sci* **7**: 748–756. doi:10.1021/acscentsci.1c00197
- Nogués MV, Moussaoui M, Boix E, Vilanova M, Ribó M, Cuchillo CM. 1998. The contribution of noncatalytic phosphate-binding subsites to the mechanism of bovine pancreatic ribonuclease A. *Cell Mol Life Sci* **54:** 766–774. doi:10.1007/s000180050205
- Ogilvie KK, Beaucage SL, Schifman AL, Theriault NY, Sadana KL. 1978. The synthesis of oligoribonucleotides. II. The use of silyl protecting groups in nucleoside and nucleotide chemistry. VII. Can J Chem **56:** 2768–2780. doi:10.1139/v78-457
- Onufriev A, Bashford D, Case DA. 2004. Exploring protein native states and large-scale conformational changes with a modified generalized Born model. *Proteins* **55:** 383–394. doi:10.1002/prot .20033
- Parr CJC, Wada S, Kotake K, Kameda S, Matsuura S, Sakashita S, Park S, Sugiyama H, Kuang Y, Saito H. 2020. N¹-Methylpseudouridine substitution enhances the performance of synthetic mRNA switches in cells. *Nucleic Acids Res* **48:** e35. doi:10.1093/nar/gkaa070
- Pauling L. 1939. The nature of the chemical bond, pp. 58–69. Cornell University Press, Ithaca, NY.
- Penzo M, Montanaro L. 2018. Turning uridines around: role of rRNA pseudouridylation in ribosome biogenesis and ribosomal function. *Biomolecules* 8: 38. doi:10.3390/biom8020038
- Potenza N, Salvatore V, Migliozzi A, Martone V, Nobile V, Russo A. 2006. Hybridase activity of human ribonuclease-1 revealed by a real-time fluorometric assay. *Nucleic Acids Res* **34:** 2906–2913. doi:10.1093/nar/gkl368

- Prasad S, Tantillo DJ. 2021. Substituent effects on the basicity of patriscabrin A and lettucenin A: evolution favors the aromatic? ACS Omega 6: 29685–29691. doi:10.1021/acsomega.1c04051
- Prats-Ejarque G, Blanco JA, Salazar VA, Nogués VM, Moussaoui M, Boix E. 2019. Characterization of an RNase with two catalytic centers. Human RNase6 catalytic and phosphate-binding site arrangement favors the endonuclease cleavage of polymeric substrates. *Biochim Biophys Acta* **1863**: 105–117. doi:10.1016/j.bbagen .2018.09.021
- Raines RT. 1998. Ribonuclease A. *Chem Rev* **98:** 1045–1066. doi:10 .1021/cr960427h
- Rajamani R, Good AC. 2007. Ranking poses in structure-based lead discovery and optimization: current trends in scoring function development. *Curr Opin Drug Discov Devel* **10**: 308–315.
- Rastelli G, Del Rio A, Degliesposti G, Sgobba M. 2010. Fast and accurate predictions of binding free energies using MM-PBSA and MM-GBSA. J Comput Chem 31: 797–810. doi:10.1002/jcc.21372
- Ressler VT, Mix KA, Raines RT. 2019. Esterification delivers a functional enzyme into a human cell. ACS Chem Biol 14: 599–602. doi:10.1021/acschembio.9b00033
- Roe DR, Cheatham TE III. 2013. PTRAJ and CPPTRAJ: software for processing and analysis of molecular dynamics trajectory data. *J Chem Theory Comput* 9: 3084–3095. doi:10.1021/ct400341p
- Roy RN, Bice J, Greer J, Carlsten JA, Smithson J, Good WS, Moore CP, Roy LN, Kuhler KM. 1997. Buffers for the physiological pH range: acidic dissociation constants of zwitterionic compounds (ACES and CHES) in water from 5 to 55°C. J Chem Eng Data 42: 41–44. doi:10.1021/je960279s
- Sahin U, Karikó K, Tureci O. 2014. mRNA-based therapeutics—developing a new class of drugs. *Nat Rev Drug Discov* **13:** 759–780. doi:10.1038/nrd4278
- Schwartz S, Bernstein DA, Mumbach MR, Jovanovic M, Herbst RH, León-Ricardo BX, Engreitz JM, Guttman M, Satija R, Lander ES. 2014. Transcriptome-wide mapping reveals widespread dynamic-regulated pseudouridylation of ncRNA and mRNA. *Cell* 159: 148–162. doi:10.1016/j.cell.2014.08.028
- Sorrentino S. 1998. Human extracellular ribonucleases: multiplicity, molecular diversity and catalytic properties of the major RNase types. *Cell Mol Life Sci* **54:** 785–794. doi:10.1007/s000180050207
- Sorrentino S. 2010. The eight human "canonical" ribonucleases: molecular diversity, catalytic properties, and special biological actions of the enzyme proteins. *FEBS Lett* **584:** 2194–2200. doi:10.1016/j .febslet.2010.04.018
- Spenkuch F, Motorin Y, Helm M. 2014. Pseudouridine: still mysterious, but never a fake (uridine)! RNA Biol 11: 1540–1554. doi:10.4161/ 15476286.2014.992278
- Stowell JK, Widlanski TS, Kutateladze TG, Raines RT. 1995. Mechanism-based inactivation of ribonuclease A. *J Org Chem* **60:** 6930–6936. doi:10.1021/jo00126a051
- Sun D, Han C, Sheng J. 2022. The role of human ribonuclease A family in health and diseases: a systematic review. *iScience* **25**: 105284. doi:10.1016/j.isci.2022.105284
- Svitkin YV, Cheng YM, Chakraborty T, Presnyak V, John M, Sonenberg N. 2017. N¹-Methyl-pseudouridine in mRNA enhances translation through eIF2α-dependent and independent mechanisms by increasing ribosome density. *Nucleic Acids Res* **45**: 6023–6036. doi:10.1093/nar/gkx135
- Thompson JE, Raines RT. 1994. Value of general acid-base catalysis to ribonuclease A. J Am Chem Soc 116: 5467–5468. doi:10.1021/ja00091a060
- Thompson JE, Venegas FD, Raines RT. 1994. Energetics of catalysis by ribonucleases: fate of the 2',3'-cyclic phosphodiester intermediate. *Biochemistry* **33:** 7408–7414. doi:10.1021/bi00189a047

- Thompson JE, Kutateladze TG, Schuster MC, Venegas FD, Messmore JM, Raines RT. 1995. Limits to catalysis by ribonuclease A. Bioorg Chem 23: 471–481. doi:10.1006/bioo.1995.1033
- Trott O, Olson AJ. 2010. AutoDock Vina: improving the speed and accuracy of docking with a new scoring function, efficient optimization, and multithreading. *J Comput Chem* **31:** 455–461. doi:10.1002/jcc.21334
- Tsui V, Case DA. 2000. Theory and applications of the generalized Born solvation model in macromolecular simulations. *Biopolymers* **56:** 275–291. doi:10.1002/1097-0282(2000)56:4<275::AID-BIP10024>3.0.CO;2-E
- Vanquelef E, Simon S, Marquant G, Garcia E, Klimerak G, Delepine JC, Cieplak P, Dupradeau F-Y. 2011. R.E.D. server: a web service for deriving RESP and ESP charges and building force field libraries for new molecules and molecular fragments. *Nucleic Acids Res* **39:** W511–W517. doi:10.1093/nar/gkr288
- Vogel AB, Kanevsky I, Che Y, Swanson KA, Muik A, Vormehr M, Kranz LM, Walzer KC, Hein S, Guler A, et al. 2021. BNT162b vaccines protect rhesus macaques from SARS-CoV-2. *Nature* **592**: 283–289. doi:10.1038/s41586-021-03275-y
- Wang J, Wolf RM, Caldwell JW, Kollman PA, Case DA. 2004. Development and testing of a general amber force field. *J Comput Chem* **25**: 1157–1174. doi:10.1002/jcc.20035
- Wang E, Sun H, Wang J, Wang Z, Liu H, Zhang JZH, Hou T. 2019. End-point binding free energy calculation with MM/ PBSA and MM/GBSA: strategies and applications in drug design. *Chem Rev* **119:** 9478–9508. doi:10.1021/acs.chemrev.9b00055
- Wang Y, Zhang Z, Luo J, Han X, Wei Y, Wei X. 2021. mRNA vaccine: a potential therapeutic strategy. Mol Cancer 20: 33. doi:10.1186/ s12943-021-01311-z
- Webb B, Sali A. 2016. Comparative protein structure modeling using MODELLER. *Curr Protoc Bioinformatics* **54:** 5.6.1–5.6.37. doi:10.1002/cpbi.3
- Weissman D, Ni H, Scales D, Dude A, Capodici J, McGibney K, Abdool A, Isaacs SN, Cannon G, Kariko K. 2000. HIV gag mRNA transfection of dendritic cells (DC) delivers encoded antigen to MHC class I and II molecules, causes DC maturation, and induces a potent human in vitro primary immune response. J Immunol 165: 4710–4717. doi:10.4049/jimmunol.165.8.4710
- Witzel H, Barnard EA. 1962. Mechanism and binding sites in the ribonuclease reaction II. Kinetic studies of the first step of the reaction. *Biochem Biophys Res Commun* 7: 295–299. doi:10.1016/0006-291X(62)90194-8
- Wlodawer A, Miller M, Sjölin L. 1983. Active site of RNase: neutron diffraction study of a complex with uridine vanadate, a transition-state analog. *Proc Natl Acad Sci* **1983:** 3628–3631. doi:10.1073/pnas
- Wurm JP, Griese M, Bahr U, Held M, Heckel A, Karas M, Soppa J, Wöhnert J. 2012. Identification of the enzyme responsible for N¹-methylation of pseudouridine 54 in archaeal tRNAs. RNA **18**: 412–420. doi:10.1261/rna.028498.111
- Ylilauri M, Pentikäinen OT. 2013. MMGBSA as a tool to understand the binding affinities of filamin-peptide interactions. *J Chem Inf Model* **53:** 2626–2633. doi:10.1021/ci4002475
- Zegers I, Maes D, Dao-Thi M-H, Poortmans F, Palmer R, Wyns L. 1994.
 The structures of RNase A complexed with 3'-CMP and d(CpA): active site conformation and conserved water molecules. *Protein Sci* 3: 2322–2339. doi:10.1002/pro.5560031217
- Zgarbova M, Otyepka M, Sponer J, Mladek A, Banas P, Cheatham TE III, Jurecka P. 2011. Refinement of the Cornell et al. nucleic acids force field based on reference quantum chemical calculations of glycosidic torsion profiles. *J Chem Theory Comput* 7: 2886–2902. doi:10.1021/ct200162x

Zhao Y, Truhlar DG. 2008a. Density functionals with broad applicability in chemistry. Acc Chem Res **41:** 157–167. doi:10.1021/ar700111a

Zhao Y, Truhlar DG. 2008b. The M06 suite of density functionals for main group thermochemistry, thermochemical kinetics, noncovalent interactions, excited states, and transition elements: two

new functionals and systematic testing of four M06-class functionals and 12 other functionals. *Theor Chem Acc* **120:** 215–241. doi:10.1007/s00214-007-0310-x

Zhou Z, Madura JD. 2004. Relative free energy of binding and binding mode calculations of HIV-1 RT inhibitors based on dock-MM-PB/GS. *Proteins* **57**: 493–503. doi:10.1002/prot.20223

MEET THE FIRST AUTHORS







Bjarne Silkenath



Volga Kojasoy

Meet the First Author(s) is an editorial feature within RNA, in which the first author(s) of research-based papers in each issue have the opportunity to introduce themselves and their work to readers of RNA and the RNA research community. Clair S. Gutierrez, Bjarne Silkenath, and Volga Kojasoy are co-first authors of this paper, "Pseudouridine residues as substrates for serum ribonucleases." Clair is a PhD student at MIT in the lab of Professor Ron Raines, working on the biochemistry of ribonucleases. Bjarne and Volga are postdoctoral fellows working with Professor Raines.

What are the major results described in your paper, and how do they impact this branch of the field?

We investigated pseudouridine (Ψ) and N^1 -methylpseudouridine ($m^1\Psi$) as substrates for pancreatic-type ribonucleases (ptRNases). We found that RNase 1 (human) and RNase A (bovine) catalyze the cleavage of UpA up to 10-fold more efficiently than the cleavage of Ψ pA or $m^1\Psi$ pA. X-ray crystallography and molecular dy-

namics simulations of enzyme·dinucleotide complexes showed that U, Ψ , and $m^1\Psi$ bind to both ptRNases in a similar manner. Quantum chemistry calculations suggested that the higher reactivity of UpA is intrinsic, arising from an inductive effect that decreases the p K_a of the 2'-hydroxy group of U and enhances its nucleophilicity toward the P–O5" bond. This study expands our understanding of the most common post-transcriptional modification in natural RNA and informs the development of RNA-based vaccines and therapeutic agents.

What led you to study RNA or this aspect of RNA science?

CSG: I was primarily interested in protein chemistry, for which ptRNases are a great model system. It was a natural step for me to look at how RNA modifications impact binding and catalysis of these proteins.

BS: My background is in carbohydrate chemistry, so when the opportunity presented itself to utilize this background in the synthesis and study of oligonucleotides, I was naturally intrigued. This intersection of disciplines allowed me to explore the intricate relationships between carbohydrates and RNA, particularly in how modifications to oligonucleotides can impact their stability and functionality.

VK: I was intrigued by the chemical diversity of RNA modifications and how they represent a significant breakthrough in advancing our understanding of RNA biology.

During the course of these experiments, were there any surprising results or particular difficulties that altered your thinking and subsequent focus?

We found that pseudouridines are at some level resistant to cleavage by ptRNases, which wasn't surprising, but that this was due to a change in catalysis rate rather than binding was surprising. To answer this, we developed and tested a hypothesis about how the $\beta\text{-}C\text{-}glycosidic}$ bond in pseudouridines impacts the pKa of the 2′ OH, which made this story more interesting.

What are some of the landmark moments that provoked your interest in science or your development as a scientist?

CSG: In my high school biology course, the section on biochemistry, which built an understanding of life from the molecular level, had me hooked.

BS: The rapid advancements in RNA research over the past few years have captivated my attention. Witnessing breakthroughs in

Continued

RNA-based therapies and their potential to revolutionize medicine has reinforced my fascination with this field.

VK: During my studies, collaborative projects with scientists from diverse backgrounds significantly helped deepen my curiosity and appreciation for innovation in research.

If you were able to give one piece of advice to your younger self, what would that be?

CSG: Read the literature deeply and broadly. Deeply to be the expert in your problem space and broadly to find creative approaches and new relationships.

BS: If you don't know something, just ask! There are so many amazing scientists around you who are more than willing to help and grow with you. Embracing curiosity and seeking guidance can open doors to new opportunities and insights that you might not have considered

VK: Always keep learning, stay adaptable, and view challenges as opportunities for growth.

Are there specific individuals or groups who have influenced your philosophy or approach to science?

CSG: My family always fostered my curiosity and exploration as long as I didn't use my younger sister as a test subject. My mentors Dr. Jake Brunkard and Dr. George Chao taught me not only how to be a careful and methodical scientist but also the importance of mentorship.

BS: Here, I must name parents and chemistry school teachers who allowed me to develop into a curious and creative chemist. Both nurtured my inquisitive nature and instilled confidence in me, which has been crucial throughout my scientific journey.

VK: The encouragement of my family has built a deep passion for lifelong learning, and my mentors and advisors throughout my ac-

ademic journey have nurtured my curiosity and creativity, profoundly shaping my scientific path.

What are your subsequent near- or long-term career plans?

 $\mbox{\bf CSG:}\mbox{\bf I}$ am planning to focus on more computational approaches to biochemistry in a postdoc.

BS: I recently made the transition from academia to industry and will focus on drug discovery

VK: I will focus on drug discovery, which I am passionate about.

What were the strongest aspects of your collaboration as co-first authors?

This collaboration was in our opinion a perfect one. We all brought very different skill sets (biological, synthetic, and computational chemistry) to the table and advanced a project that none of us could have done alone.

How did you decide to work together as co-first authors?

CSG: On my first day back in the lab from parental leave, our PI, Ron, asked me to meet with two new postdocs in the lab for a project looking at pseudouridines as substrates for ptRNases. I'm so fortunate he did, as Bjarne and Volga are amazing scientists who have taught me so much in this project and beyond!

BS: Again, it was the different backgrounds that brought us together, and I am very thankful that I was able to work with and learn from these great scientists.

VK: Our advisor brought us together for this project, and I feel so lucky to have worked with such incredibly talented scientists from diverse backgrounds. I truly enjoyed discussing science and learning from them.